Inorganic Chemistry

Article

pubs.acs.org/IC

Half-Sandwich Complexes of Dy^{III}: A Janus-Motif with Facile Tunability of Magnetism

Shan-Shan Liu, Ling Xu, Shang-Da Jiang, Yi-Quan Zhang, Yin-Shan Meng, Zitao Wang, Bing-Wu Wang,* Wen-Xiong Zhang,* Zhenfeng Xi, and Song Gao*

Beijing National Laboratory for Molecular Sciences, State Key Laboratory of Rare Earth Materials Chemistry and Applications, College of Chemistry and Molecular Engineering, Peking University, No. 5 Yiheyuan Road, Beijing 100871, China

Supporting Information

ABSTRACT: Three half-sandwich organometallics $[(Cp^R)Dy(DBM)_2(THF)]$·solvent [Cp^R = Cp* (**1Dy**, Cp* = C_5Me_5), Cp^{4PrPh} (**2Dy**, Cp^{4PrPh} = C_5Pr_4Ph), Cp′ (**3Dy**, Cp′ = C_5Me_4TMS, solvent = THF), DBM^- = dibenzoylmethanoate anion, THF = tetrahydrofuran, TMS = trimethylsilyl] with a Janus structural motif, where the ligands of DBM^- and $[Cp^R]^-$ are widely used in Dy^{III}/β-diketonate and Ln^{III}/cyclopentadienyl systems, were synthesized, structurally and magnetically characterized, and theoretically investigated. Single-crystal structural analysis reveals that the three complexes crystallize in the same space group $P2_1/c$. All the molecules display slow magnetic relaxation in the absence of an applied magnetic field, and the magnetic hysteresis loops of **2Dy** and **3Dy** can be observed under a magnetic field sweep rate of 10 Oe/s, indicating all three complexes are single-ion magnets (SIMs). The modifications of the Cp-ring lead to the distinct increment of the energy barrier from 46 K (**1Dy**) to 76 K (**2Dy**) to 320 K (**3Dy**). *Ab initio* calculations show that the ground Kramers doublet is strongly axial with g_z approaching the value of 20 expected for the pure $M_J = \pm 15/2$ state, and the magnetic anisotropy axes for three complexes share a similar orientation which is perpendicular to the molecular pseudosymmetric axis. Electrostatic analyses confirm the magnetic anisotropy orientations and reveal that proper charge distribution of the coordination sphere (including the first and second) around Dy^{III} ion enhances the magnetic anisotropy. Further investigation of the relaxation mechanisms suggests the energy barrier should be carefully used to evaluate single-ion magnets if Raman process is dominant in the low temperature range.

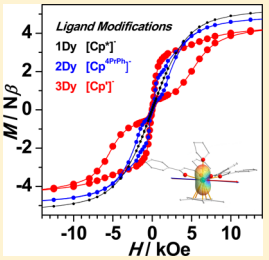

INTRODUCTION

Single-ion magnets (SIMs), which contain only one paramagnetic ion in the molecule, show magnetic bistability below a certain temperature, originating from the anisotropy of a single metallic ion rather than magnetic coupling between paramagnetic centers present in multinuclear single-molecule magnets (SMMs).[1] The absence of magnetic interaction simplifies the understanding and control of the magnetic anisotropy which is of crucial importance in designing molecular magnetic materials. In the past decade, lanthanide based SIMs have drawn wide attention because of their promising magnetic anisotropy due to the largely residual orbital angular momentum in a crystal field.[2] In particular, Tb^{III}/ Dy^{III}/ Ho^{III}/ Er^{III} ions are commonly used in the reported SIMs, of which Dy^{III}-SIMs account for the largest number.[3]

The ligand modification is an effective approach to tune the relaxation energy barrier and blocking temperature, since the slow magnetic relaxation of 4f based SIMs is extremely sensitive to the low lying states of lanthanide ions.[4] One example is the Dy^{III}/β-diketonate[5] system in which various ligand modifications have been well-investigated, and some of them achieved remarkable improvements in terms of magnetic properties. The energy barrier was considerably enhanced by replacing the ligand $acac^-$ (acac = acetylacetonate) with tta^- (tta = 1-(2-thiophenyl)-3-trifluoromethylacetylacetonate) in the complex $[Dy(acac)_3(1,10\text{-phen})]$.[5b,d] Modifying the neutral ligand can also lead to a similar enhancement; that is, the energy barrier increased from 64 K ($[Dy(acac)_3(1, 10\text{-phen})]$) to 187 K ($[Dy(acac)_3(dppz)]$, dppz = dipyrido[3,2-*a*:2′,3′-*c*]-phenazine).[5f] Recently, another organometallic SIM system, Ln^{III}/cyclomultiene[6] (cyclomultiene = carbocyclic cyclopentadienyl, cyclooctatetraenyl, arene, etc.) complexes, has attracted considerable interest since the first organometallic SIM $[(COT)Er(Cp^*)]$[6a] (COT^{2-} = cyclooctatetraenide dianion, $[Cp^*]^-$ = pentamethylcyclopentadienide anion) was characterized by Gao et al. This type of organolanthanide complexes exhibits great potential for discovering SIMs with superior molecular magnetic properties. A large coercivity of 7 kOe was obtained in $[Er(COT)_2]^-$.[6c,d] $[Cp^*_2Dy(BPh_4)]$ displays the energy barrier of 473 K which is the highest among all Dy^{III}-SIMs so far.[6e] However, unlike the Dy^{III}/β-diketonate system where the fine-tuning of the ligand environment has been widely used and has proven to be a valuable method to enhance the magnetic properties, systematic ligand modifications of Dy^{III}/cyclomultiene SIMs have rarely been studied probably due to the challenges of synthesis and maintaining the molecular geometry while tuning the ligand structure. Attracted by the outstanding magnetic behavior of β-diketonate and

Received: November 13, 2014
Published: May 20, 2015

DOI: 10.1021/ic502734z
Inorg. Chem. 2015, 54, 5162−5168

cyclopentadienyl based Dy^{III}-SIMs, we designed and synthesized a half-sandwich Dy^{III} complex with a Janus structural motif by using dibenzoylmethanoate and pentamethylcyclopentadienyl ligands which are popular in the two aforementioned systems, and further modified the substituent groups of the cyclopentadienyl ligand to tune the magnetic anisotropy and investigate the magneto-structural relationship.

Herein we report the syntheses of a group of half-sandwich complexes, $[(Cp^*)Dy(DBM)_2(THF)]$ (**1Dy**, Cp^* = C_5Me_5), $[(Cp^{4PrPh})Dy(DBM)_2(THF)]$ (**2Dy**, Cp^{4PrPh} = C_5Pr_4Ph), $[(Cp')Dy(DBM)_2(THF)](THF)$ (**3Dy**, Cp′ = C_5Me_4TMS), where DBM^- is dibenzoylmethanoate anion and TMS is trimethylsilyl. The magnetic studies reveal that all three complexes behave as SIMs, and the subsequent analysis of magnetic results shows that the presence of a Si atom on the aromatic ring in **3Dy** leads to an obvious improvement of the magnetic relaxation barrier and blocking temperature in comparison to **1Dy** and **2Dy**, revealing the powerful role of chemical design played in magnetism. *Ab initio* calculations were also performed, and the magnetic easy axes of these molecules are perpendicular to the molecular pseudosymmetric axis, which is in accordance with the electrostatic analyses.

EXPERIMENTAL SECTION

General Methods. All reactions were conducted under a slightly positive pressure of dry nitrogen using standard Schlenk line techniques or under a nitrogen atmosphere in a Vigor (SG 1200/750TS-F) glovebox. The nitrogen in the glovebox was constantly circulated through a copper/molecular sieves catalyst unit. The oxygen and moisture concentrations in the glovebox atmosphere were monitored by an O_2/H_2O Combi-Analyzer to ensure both were always below 1 ppm. Unless otherwise noted, all starting materials were commercially available and were used without further purification. Solvents were purified by an Mbraun SPS-800 solvent purification system and dried over fresh Na chips in the glovebox. *n*-BuLi was obtained from J&K. Elemental Analysis was conducted on Elementar Vario MICRO CUBE (Germany).

Preparation of [Cp*Dy(DBM)$_2$(THF)] (1Dy). As described in Scheme 1, 20 mL of THF solution of $DyBz_3$ (Bz = $CH_2C_6H_4$-*o*-NMe_2)

Scheme 1. Schematic Representation of the Synthesis of 1Dy

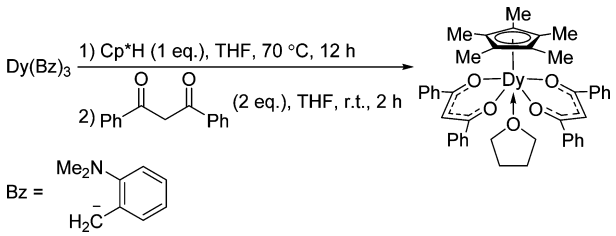

(565.1 mg, 1.000 mmol), which was prepared according to the literature procedure,[7] was added in a 25 mL Schlenk tube in glovebox. Then Cp*H (136.2 mg, 1.000 mmol) was added in this tube, and the sealed Schlenk tube was taken outside the glovebox. The mixture was stirred at 70 °C for 12 h. When the tube was cooled to room temperature, it was taken inside the glovebox, and THF was moved under reduced pressure. Hexane (3 mL) was added to extract HBz out. Then, the hexane layer was moved out, and the residue solvent was evaporated to give yellow powder. When dibenzoylmethane (DBM) (390.2 mg, 1.740 mmol, dissolved in 5 mL THF) was added to THF solution (15 mL) of this powder, the color of reaction mixture turned to red immediately. Also, the mixture was stirred for another 2 h in glovebox. After removal of THF under reduced pressure, the residue was extracted by hexane (5 mL) to remove HBz. Then, the hexane layer was decanted, and residual solid was dried up under vacuum to give **1Dy** as dark red powder (696.3 mg, 85% yield). A single crystal suitable for X-ray diffraction and magnetic analysis could be grown from THF/hexane (5 mL/5 mL) at −20 °C. Anal. Calcd for $C_{44}H_{45}O_5Dy$: C, 64.74; H, 5.56. Found: C, 64.52; H, 5.53.

Preparation of [Cp^{4PrPh}Dy(DBM)$_2$(THF)] (2Dy). $Cp^{4PrPh}H$ was prepared by $AlCl_3$ mediated reaction of tetrapropylzirconacyclopentadiene with benzaldehyde.[8] As described in Scheme 2, after $Cp^{4PrPh}Li$

Scheme 2. Schematic Representation of the Synthesis of 2Dy

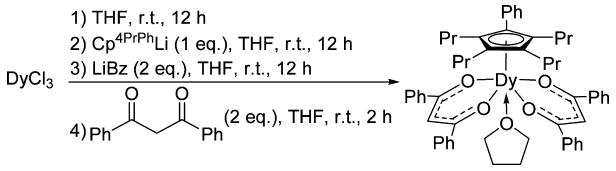

(316.4 mg, 1.000 mmol), which was generated from $Cp^{4PrPh}H$ and *n*-BuLi, was treated with a suspension of $DyCl_3$ (268.9 mg, 1.000 mmol) in THF at room temperature for 12 h, LiBz (282.2 mg, 2.000 mmol, dissolved in 5.0 mL THF) was added to the reaction mixture and stirred for another 12 h at room temperature. Then, THF was removed under reduced pressure, and the residue was extracted by toluene. After LiCl was filtered, the toluene from the filtrate was removed under reduced pressure, and 15 mL of THF was added to give a yellow solution. When DBM (179.4 mg, 0.80 mmol) was added to this solution, the color of the reaction mixture turned to red immediately. Also, the mixture was stirred for another 2 h. After removal of THF under reduced pressure, the residue was extracted by hexane (5 mL) to remove HBz. Then, the hexane layer was decanted, and residual solid was dried under vacuum to give **2Dy** as red powder (370.3 mg, 37% yield).[7c] Single crystals suitable for X-ray diffraction and magnetic analysis could be grown from THF/hexane (5 mL/5 mL) at −20 °C. Anal. Calcd for $C_{57}H_{63}O_5Dy$: C, 69.11; H, 6.41. Found: C, 68.64; H, 6.68.

Preparation of [Cp′Dy(DBM)$_2$(THF)]·THF (3Dy). As described in Scheme 3, 20 mL of THF solution of $DyBz_3$ (Bz = $CH_2C_6H_4$-*o*-NMe_2)

Scheme 3. Schematic Representation of the Synthesis of 3Dy

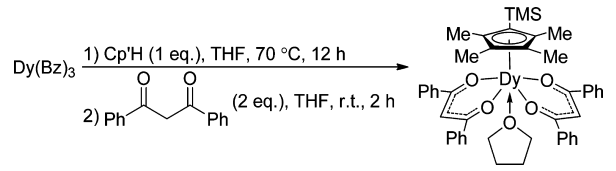

(565.1 mg, 1.000 mmol), which was prepared according to the literature procedure,[7] was added to a 25 mL Schlenk tube in glovebox. Then Cp′H (194.4 mg, 1.000 mmol) was added in this tube, and the sealed Schlenk tube was taken outside the glovebox. The mixture was stirred at 70 °C for 12 h. When the tube was cooled to room temperature, it was taken inside the glovebox, and THF was moved under reduced pressure. Hexane (3 mL) was added to extract HBz out. Then, the hexane layer was moved out, and the residue solvent was evaporated to give yellow powder. When DBM solution (296.1 mg, 1.32 mmol, dissolved in 5 mL THF) was added to THF solution (15 mL) of this powder, the color of the reaction mixture turned to red immediately. Also, the mixture was stirred for another 2 h in the glovebox. After removal of THF under reduced pressure, the residue was extracted by hexane (5 mL) to remove HBz. Then, the hexane layer was decanted, and residual solid was dried up under vacuum to give **3Dy** as red powder (530.9 mg, yield: 61%). Single crystals suitable for X-ray diffraction and magnetic analysis could be grown from THF/hexane (5 mL/5 mL) at −20 °C. Anal. Calcd for $C_{50}H_{59}O_6SiDy$: C, 63.44; H, 6.28. Found: C, 63.13; H, 6.06.

Crystal Structure Determination. The single crystals of **1Dy**, **2Dy**, and **3Dy** suitable for X-ray analysis were grown as shown in the Experimental Section. These crystals were manipulated under a

DOI: 10.1021/ic502734z
Inorg. Chem. 2015, 54, 5162−5168

nitrogen atmosphere and were sealed in a thin-walled glass capillary. Data collections for **1Dy** and **3Dy** were performed at 173 K on an Aglient technologies Super Nova Atlas Dual System, with a (Mo Kα = 0.710 73 Å) microfocus source and focusing multilayer mirror optics. Measurement of **2Dy** was performed at 173 K on a RIGAKU CCD SATURN 724 diffractometer, using graphite-monochromated Mo Kα radiation (λ = 0.710 73 Å). The determination of crystal class and unit cell parameters was carried out by the CrysAlisPro[9] program for **1Dy** and **3Dy** or Crystal Clear (RigakuInc., 2007) for **2Dy**. The raw frame data were processed using the CrysAlisPro[9] program for **1Dy** and **3Dy** or Crystal Clear (RigakuInc., 2007) for **2Dy** to yield the reflection data file. Using Olex2,[10] the structures of **1Dy** were solved with the Superflip[11] structure solution program using Charge Flipping and refined with the ShelXL[12] refinement package using least squares minimization; the structures of **2Dy** and **3Dy** were solved by use of the SHELXTL program.[13] Refinement was performed on F^2 anisotropically for all the non-hydrogen atoms by the full-matrix least-squares method. The hydrogen atoms were placed at the calculated positions and were included in the structure calculation without further refinement of the parameters. Disordered solvent in **2Dy** was squeezed by using Platon.[14] Crystallographic data (excluding structure factors) have been deposited with the Cambridge Crystallographic Data Centre as supplementary publication nos. 1021907−1021909. Copies of these data can be obtained free of charge from the Cambridge Crystallographic Data Centre via www.ccdc.cam.ac.uk/data_request/cif. Crystal data, data collection, and processing parameters for the complexes **1Dy**, **2Dy**, and **3Dy** are summarized in Table 1.

Table 1. Crystallographic Data and Structure Refinements for 1Dy, 2Dy, and 3Dy

	1Dy	2Dy	3Dy
formula	$C_{44}H_{45}O_5Dy$	$C_{57}H_{63}O_5Dy$	$C_{50}H_{59}O_6SiDy$
fw	816.30	990.57	946.56
cryst syst	monoclinic	monoclinic	monoclinic
space group	$P2_1/c$	$P2_1/c$	$P2_1/c$
a, Å	14.1877(4)	13.822(3)	19.5489(7)
b, Å	12.2396(4)	16.192(3)	14.1446(3)
c, Å	24.4095(8)	23.408(5)	18.4719(7)
β, deg	119.265(2)	105.43(3)	116.390(5)
V, Å^3	3697.8(2)	5050.0(18)	4575.4(3)
Z	4	4	4
T, K	173(2)	173(2)	173(2)
F(000)	1660	2044	1948
μ, mm^{-1}	2.066	1.525	1.706
λ, Å	0.710 73	0.710 73	0.710 73
R1 [$I \geq 2\sigma(I)$]	0.0328	0.0587	0.0323
wR2 (all data)	0.0725	0.1171	0.0753
S	1.010	1.179	1.037

Magnetic Properties Measurements. The sample was fixed on the middle plate of the symmetrical and joint NMR tube with eicosane and parafilm to avoid movement during the measurements. The NMR tube was sealed in vacuum to protect samples from air. Direct current magnetism and ac properties of polycrystalline powder samples were performed on a Quantum Design MPMS XL-5 SQUID magnetometer. Magnetic data were corrected with eicosane, parafilm, NMR tube, and Pascal constants.

***Ab Initio* Calculations.** Complete-active-space self-consistent field (CASSCF) calculations on individual lanthanide fragments have been carried out with MOLCAS 7.8 program package.[15] In all calculations, we used the complete structures of three Dy complexes shown in Figure 1 and Supporting Information Figure S1. The basis sets for all atoms are atomic natural orbitals from the MOLCAS ANO-RCC library: ANO-RCC-VTZP for Dy(III) ion; VTZ for close O and C; VDZ for distant atoms. The calculations employed the second order Douglas−Kroll−Hess Hamiltonian, where scalar relativistic contractions were taken into account in the basis set and the spin−orbit coupling was handled separately in the restricted active space state interaction (RASSI-SO) procedure. For each complex, the active electrons in 7 active spaces include all nine f electrons (CAS(9 in 7)) in the CASSCF calculation. To exclude all doubts, we calculated all the roots in the active space. We have mixed the maximum number of spin-free states which was possible with our hardware (all from 21 sextets; 128 from 224 quadruplets; 130 from 490 doublets).

RESULTS AND DISCUSSION

Crystallography. Single-crystal X-ray diffraction investigation shows that **1Dy**, **2Dy**, and **3Dy** crystallize in the monoclinic space group $P2_1/c$. Selected crystallographic data are shown in Table 1. The three complexes differ in the substituents on the aromatic ring. The ring ligand of **1Dy** is 1,2,3,4,5-pentamethylcyclopentadienide anion ($[Cp^*]^-$), while the methyl groups are substituted by four propyl groups and one phenyl group for **2Dy,** named $[Cp^{4PrPh}]^-$; only one methyl group of $[Cp^*]^-$ is substituted by a trimethylsilyl group for **3Dy**, and it is labeled as $[Cp']^-$. Nevertheless, these substituents do not change the coordination mode of this series. The Dy^{III} ion is capped by the aromatic ring from one side and chelated by two DBM^- ligands from the other side. One neutral THF molecule coordinates to the central ion between the DBM^- ligands. The structure of **1Dy** is shown in Figure 1 (see structures of **2Dy** and **3Dy** in Supporting Information Figure S1). This sort of ligand combination provides a 2-fold symmetry environment. Also, the molecular pseudosymmetric axis is along the Dy^{III}−centroid (Cp-ring) direction. A detailed comparison of three structures reveals that the angles between two DBM^- ligands (α and β labeled in Figure 1) are 80.7°/114.7° for **1Dy**, 90.1°/102.6° for **2Dy**, and 89.1°/102.4° for **3Dy**, indicating the lower symmetry of **1Dy**.

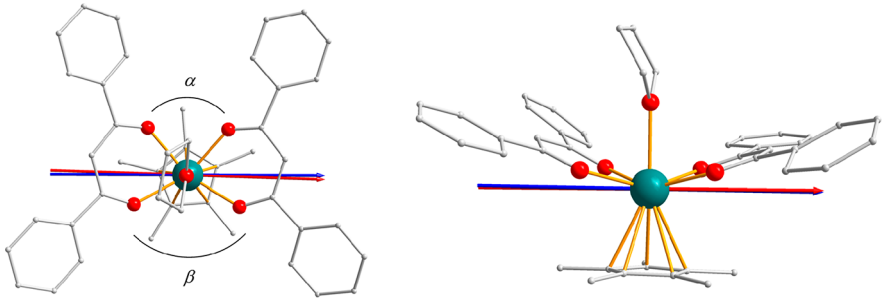

Figure 1. Crystal structures of **1Dy** viewed parallel (left) and perpendicular (right) to the pseudomolecular axis. The red and blue arrows represent the calculated easy axis by *ab initio* and electrostatic methods, respectively (see the text). α and β indicate the angles between two DBM^- ligands. Color code: dysprosium (teal), oxygen (red), carbon (gray). Hydrogen atoms are omitted for clarity.

DOI: 10.1021/ic502734z
Inorg. Chem. 2015, 54, 5162−5168

The shortest distance between two Dy^{III} ions in the lattice is 8.7498(4) Å for **1Dy**, 10.5024(16) Å for **2Dy**, and 9.4126(7) Å for **3Dy**, respectively. The detailed structure data for **1Dy**, **2Dy**, and **3Dy** are listed in Supporting Information Table S1.

Static Magnetic Properties. The temperature dependence of magnetic susceptibility measurements for **1Dy**, **2Dy**, and **3Dy** were performed under a 1 kOe direct current (dc) magnetic field in the temperature range from 2 to 300 K (Figure 2). The $\chi_m T$ values at 300 K are 14.08 and 14.15 emu K mol^{-1} for **1Dy** and **2Dy**, respectively, close to the value of the free Dy^{III} ion (14.17 emu K mol^{-1}, $^6H_{15/2}$). The $\chi_m T$ value of 13.15 emu K mol^{-1} for **3Dy** at 300 K is slightly smaller than the theoretical value, which might be ascribed to the fact that the states split by the crystal field within the ground Russell–Saunders multiplet are not equally populated even at room temperature since $\chi_m T$ keeps increasing upon warming near room temperature. Upon cooling, $\chi_m T$ decreases gradually until ca. 5 K and then drops rapidly to the base temperature. This should be mainly related to the depopulation of the electronic fine structures caused by crystal field effect and possible intermolecular interactions, and the sudden drop of $\chi_m T$ at low temperature suggests possible magnetic blocking.[6c,16] The M versus H plots at 2 K indicate that the three Dy^{III} complexes have the same tendency and reach the values of 5.44, 5.39, 4.49 Nβ with the static field up to 50 kOe for **1Dy**, **2Dy**, and **3Dy**, respectively (Supporting Information Figures S2–S4). The large deviation from the theoretical saturation value of 10 Nβ is attributed to the magnetic anisotropy and ligand effects at the Dy^{III} ion that eliminate the 16-fold degeneracy of the $^6H_{15/2}$ ground state.[17] The plots of M versus HT^{-1} at various temperatures cannot be superimposed (Supporting Information Figures S5–S7), which indicates the single-ion anisotropy as well.[18]

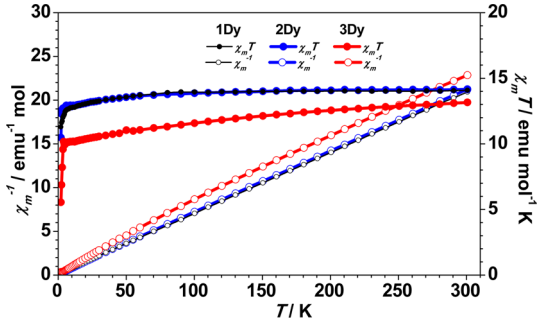

Figure 2. Temperature dependence of $\chi_m T$ and χ_m^{-1} under a 1 kOe static field at the temperature range 2–300 K for **1Dy**, **2Dy**, and **3Dy**.

Dynamic Magnetic Properties. Alternating current (ac) magnetic susceptibilities were studied at a 3 Oe oscillating ac field below 30 K in the frequency range 1–1000 Hz. Both the in-phase (χ') and out-of-phase (χ'') components of dynamic magnetic susceptibility of all the three complexes show strong frequency (ν) and temperature (T) dependence below 30 K in the absence of a static field, indicating the presence of slow magnetic relaxation associated with SIM behavior. For **1Dy**, χ'' shows frequency-dependence with only two observed peaks above 10 K (Supporting Information Figure S8). More peaks of $\chi''(T)$ can be observed for **2Dy** (Supporting Information Figure S9). Interestingly, for **3Dy** peaks are shown in all the measured frequencies (Supporting Information Figure S10), suggesting that a higher energy barrier could be expected. Accordingly, the χ'' versus ν plots for these three complexes were characterized and shown in Figure 3. χ'' becomes frequency-independent below 6 and 8 K for **1Dy** and **2Dy**, respectively, which can be defined as a crossing temperature (T_{cross}) from the thermally activated dominated relaxation to the quantum tunneling dominated mechanism upon cooling. Unlike the other two complexes, **3Dy** always exhibits frequency-dependence in the temperature range 9–22 K, indicating the largely suppressed tunneling process.

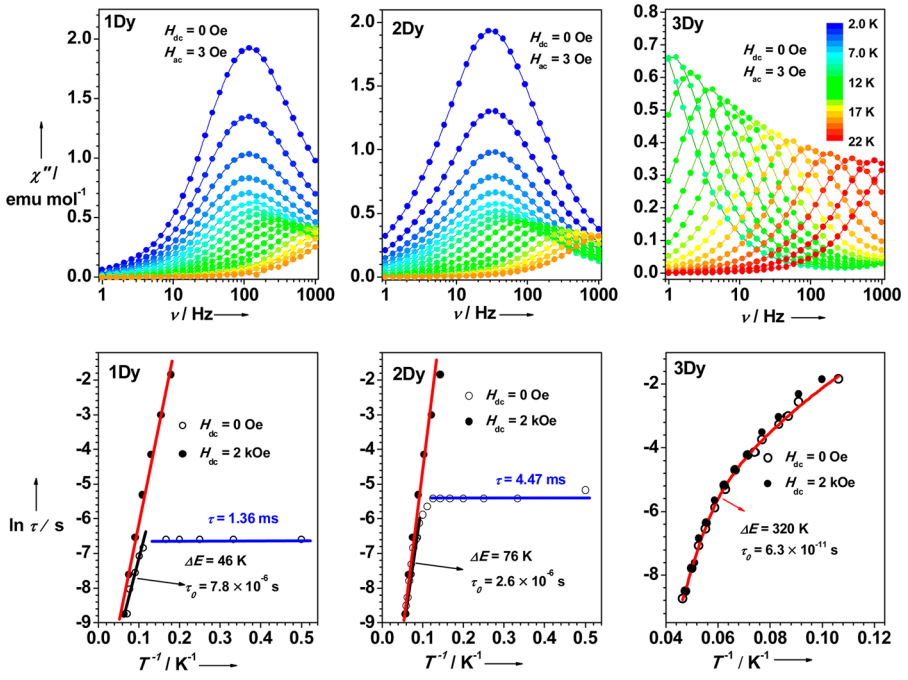

Figure 3. (Top) Plot of out-of-phase magnetic susceptibility (χ'') vs frequency (ν) at various temperatures in the absence of a static field for **1Dy**, **2Dy**, and **3Dy**. (Bottom) Plot of relaxation time (ln τ) vs T^{-1} for **1Dy**, **2Dy**, and **3Dy** under zero dc field and a 2 kOe applied dc field.

DOI: 10.1021/ic502734z
Inorg. Chem. 2015, 54, 5162–5168

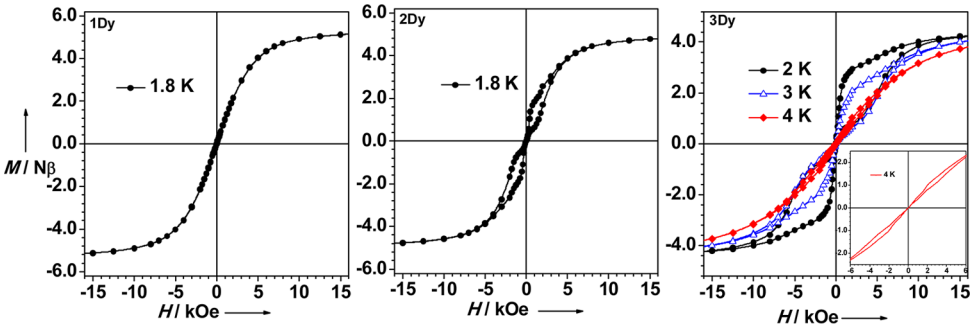

Figure 4. Magnetic hysteresis of **1Dy**, **2Dy**, and **3Dy**. The inset shows the hysteresis at 4 K for **3Dy**.

A 2 kOe static field was applied to investigate the suppression of the quantum tunneling of the magnetization (QTM) in three complexes, showing that the tails of **2Dy** and **3Dy** at low temperature disappear, while a small one of **1Dy** still remains (Supporting Information Figures S11−S13). The relaxation time (τ) of the three complexes as a function of the inverse temperature (T^{-1}) at 2 kOe is plotted in Figure 3. The tendency of ln τ versus T^{-1} of **3Dy** behaves quite differently from those of **1Dy** and **2Dy**. The applied static field does not change the relaxation behavior a lot for **3Dy**, consistent with the aforementioned largely suppressed tunneling effect.

Arrhenius analyses of the dynamic susceptibilities in the absence of a static field show that the thermally activated energy barrier is 46 K for **1Dy** with $\tau_0 = 7.8 \times 10^{-6}$ s, 76 K for **2Dy** with $\tau_0 = 2.6 \times 10^{-6}$ s, and 242 K for **3Dy** with $\tau_0 = 2.2 \times 10^{-9}$ s (Supporting Information Figure S14). However, a simple Arrhenius analysis is not suitable for **3Dy** as the ln τ versus T^{-1} plots are nonlinear under either zero field or a 2 kOe dc field (Supporting Information Figures S13 and S15). The analysis of Cole−Cole plots reveals that the distribution factor α in the generalized Debye model[19] is always smaller than 0.11, indicating a single relaxation process (Supporting Information Figure S16). A combination of the relaxation mechanisms has to be taken into account so as to understand the ln τ vs T^{-1} behavior. The direct process can be excluded since the relaxation behavior is insensitive to the applied field. The energy barrier for **3Dy** in the absence of a dc field is fitted to be 320 K with $\tau_0 = 6.3 \times 10^{-11}$ s by eq 1,[20] with the consideration of Raman (n = 6.2, $B = 4.8 \times 10^{-6}$) and Orbach processes (Figure 3). The two processes contribute equally to the overall relaxation rate around 18 K, and the Orbach process dominates in the high temperature range (T > 18 K) whereas the Raman process prevails in the low temperature range (T < 18 K) (Supporting Information Figure S17). It is noteworthy that blocking temperature is usually located in the low temperature range. For **3Dy**, the relaxation process occurs via Raman mechanism at the low temperature and Orbach mechanism at the high temperature, while the energy barrier is fitted from the Orbach process. Therefore, enhancing the barrier will not be sufficient to achieve high blocking temperature considering the fact that the relaxation process in different temperature ranges could be dominated by different mechanisms. From this perspective, the energy barrier may not be enough for the evaluation of SIMs.

$$1/\tau = BT^n + 1/\tau_0 \exp(-\Delta E/T) \quad (1)$$

As it is important behavior for SIMs, magnetic hysteresis was measured for the three complexes. The results show that the hysteresis becomes more obvious in the sequence **1Dy**, **2Dy**, and **3Dy**. At an average 10 Oe/s sweep rate of the magnetic field, **1Dy** is not able to show any hysteresis openings at 1.8 K, and **2Dy** behaves with a small butterfly shaped opening only at 1.8 K, while **3Dy** shows the largest hysteresis among this series, which can be observed up to 4 K (Figure 4).

It is noteworthy that in the magnetic quantum tunnelling regime, the magnetization reversal time of **2Dy** (τ = 4.47 ms) is longer than that of **1Dy** (τ = 1.36 ms). This confirms the more obvious hysteresis in **2Dy** than **1Dy** due to the slower relaxation behavior. These results clearly reveal the extreme sensitivity of magnetic behavior on the subtle ligand modifications.

Theoretical Analysis. To further evaluate the magnetic properties of this series of molecules, we performed post-Hartree−Fock *ab initio* calculations based on the relativistic quantum chemistry method CASSCF/RASSI/SINGLE_ANISO.[21] This approach, implemented in MOLCAS code,[T5] has already been found to be an accurate tool to predict the anisotropy of lanthanide based molecular complexes.[5j,22]

As tabulated in Table 2, the largest component of effective g tensors in the diagonalized form of the ground Kramers doublets approaches the value of 20 for all three complexes. This provides fundamental evidence of the SIM behavior. In addition, the calculated $\chi_m T$ versus T and M versus H plots match the experimental curves (Supporting Information Figures S18−20 and S2−4).

Table 2. Calculated g Values of the Ground Kramers Doublets for 1Dy, 2Dy, and 3Dy

param	1Dy	2Dy	3Dy
g_x	0.0616	0.0023	0.0019
g_y	0.1028	0.0025	0.0025
g_z	19.7267	19.8083	19.8057

The easy axis orientation of **1Dy** calculated by the *ab initio* method is shown as the schematic models in Figure 1 and 5 (see Supporting Information Figures S21 and S22 for **2Dy** and **3Dy**). The easy axes of these three molecules are perpendicular to the pseudoaxial direction of the molecule, which is similar to the result of the Dy^{III}/DOTA system where the simple magneto-structural relation fails to predict the magnetic easy axis.[22b,c] More specifically, the easy axes lie in the direction of two DBM^- ligands similar to paddle-wheel-shaped Dy^{III}/β-diketonate system.[23] To understand the orientation of the easy axis, several approaches have been developed from the standpoint of electrostatic analyses, such as SIMPRE[24] and MAGELLAN.[23] On the basis of the minimal valence bond model applied in MAGELLAN,[23] apparently the negative

DOI: 10.1021/ic502734z
Inorg. Chem. 2015, 54, 5162−5168

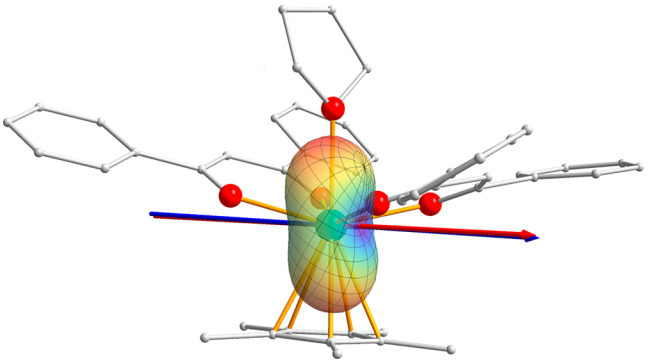

Figure 5. Schematic description of the potential energy of the system via orienting the quantized axis of $|\pm 15/2\rangle$ doublet in the Cartesian space, where red and purple represent the highest and lowest energy, respectively. The red arrow shows the g_z tensor component eigenvector direction, and the blue arrow is the minimum potential energy direction.[23] The angle between the two directions is determined to be 1.7°. All the analyses are based on the molecular structure of **1Dy**. See schemes for **2Dy** and **3Dy** in Supporting Information Figures S21 and S22.

charges on the O atoms from DBM^- are much larger than those on the C atoms from the aromatic ring and the O atom from the neutral THF molecule, where it is more capable of stabilizing the ground doublet compared to the molecular pseudoaxial direction. Since the g_z values of the calculated ground doublets in the series are very close to 20 as expected for the pure $|\pm 15/2\rangle$ state, it is reasonable to approximate the ground state electron cloud as the situation of $|\pm 15/2\rangle$, which can be considered as a linear combination of spherical harmonics up to the sixth order.[25] The electron cloud of $|\pm 15/2\rangle$ Kramers doublet shows an axial-pressed cake (oblate) shape, and the quantized axis orientation prefers the negative charge dense direction so as to stabilize the overall potential energy which could be calculated on the basis of the electrostatic method.[23] Figure 5 shows the potential surface of various orientation of the quantized axis of the $|\pm 15/2\rangle$ Kramers doublet in the Cartesian space, where red represents the highest potential while purple refers to the lowest one when the quantized axis is oriented in the corresponding direction. It is clear that the molecular pseudoaxial direction is not the preferable direction for easy axis since the potential is rather high. The minimum energy is found in the direction of the two DBM^- ligands, which is perpendicular to the molecular axis, consistent with the *ab initio* calculation results. This observation also explains the similar easy axis orientation in this series of molecules, since the major stabilization charges origin from the two β-diketonate anions, rather than the negative charges on the aromatic ring. Therefore, a slight tuning of the cyclopentadiene barely affected the molecular easy axis orientation despite the fact that it significantly enhanced the relaxation barrier.

The ligand modification effects on the magnetic properties are analyzed by the assistance of Mulliken population. Compared to **1Dy**, the phenyl substituent of **2Dy** makes the negative charges on Cp-ring delocalize onto phenyl group, resulting in a smaller charge on the Cp-ring (−0.53 for **2Dy**, −0.61 for **1Dy**). Furthermore, Dy−C(Cp) in **2Dy** has a longer bond distance (2.686 Å) than that of **1Dy** (2.649 Å) due to the steric effect of the Cp ring. These two factors decrease the repulsive potential around the equator plane of the quantized axis; thus, a larger g_z value and a smaller $g_{x,y}$ value should be present in **2Dy**. Compared to **1Dy** and **2Dy**, **3Dy** is a more complicated case. As listed in Supporting Information Table S2, the charge of the Cp-ring is larger than those of both **1Dy** and **2Dy**. Nevertheless, the positive charge on the silicon atom (+1.92) severely affects the 4f electron clouds. As a positive charge bonding to the Cp-ring, it is able to stabilize the quantized axis in the present orientation, so as to achieve a larger effective g_z value and a corresponding smaller $g_{x,y}$ value. The presence of the positively charged silicon atom along the equator plane of the quantized axis is the essence of improving the magnetic properties in **3Dy**. This observation can also be verified by the *ab initio* calculation results (Table 2). The two transverse components of the **g** tensor of **1Dy** are considerably higher than those of **2Dy** and **3Dy**, indicating the state mixing of **1Dy** is much more intensive than the other two molecules.[26] This may play a role in affecting QTM,[27] which is consistent with their magnetic behavior.

The results of *ab initio* calculations, coupled with the electrostatic analyses, reveal that decreasing the negative charge of the ligands on the magnetic hard plane of the Dy^{III} ion and increasing the bond lengths of Dy^{III} ion and those ligands are two effective approaches to enhance magnetic anisotropy. Our systematic experimental work provides evidence for the view that concentrating the major negative charges in one certain direction as much as possible leads to magnetic anisotropy.[23,26,28] Therefore, it is reasonable to believe that the magnetic behavior of Dy^{III} based mononuclear complexes with a preferable negative charge direction of the coordination sphere would be encouraging to explore.

CONCLUSIONS

In summary, we synthesized a series of half-sandwich organometallic Dy^{III}-SIMs with a Janus structural motif by using dibenzoylmethanoate and cyclopentadienyl derivatives. Interestingly, the tuning of the cyclopentadienyl ligand significantly enhances the magnetic properties, leading to a 6-fold enhancement of the energy barrier (320 K with a blocking temperature of 4 K), while the easy axis orientation is insensitive to the modification of the cyclopentadienyl ligand, as proved by *ab initio* calculations and electrostatic analyses. Further comparison of the electronic structures explains that the different electrostatics around the Dy^{III} ion gives rise to the huge difference in energy barrier and blocking temperature among the three complexes. Our systematic investigation illustrates the power of chemical tuning in controlling the electronic structure and magnetic property.

Additionally, in the case that the Raman process dominates in the low temperature range as discussed in **3Dy**, a high energy barrier may not necessarily translate into a high blocking temperature, which makes the energy barrier an inaccurate parameter to evaluate SIMs.

ASSOCIATED CONTENT

Supporting Information

Listings of crystal structures of **2Dy** and 3**Dy**, magnetic figures, Cole−Cole fitting plot, potential energy schemes and anisotropy axis orientation of **2Dy** and **3Dy**, information for selected bond lengths and angles, and CIF files of three complexes. The Supporting Information is available free of charge on the ACS Publications website at DOI: 10.1021/ic502734z.

DOI: 10.1021/ic502734z
Inorg. Chem. 2015, 54, 5162−5168

AUTHOR INFORMATION

Corresponding Authors

*E-mail: wangbw@pku.edu.cn.
*E-mail: wx_zhang@pku.edu.cn.
*E-mail: gaosong@pku.edu.cn.

Notes

The authors declare no competing financial interest.

ACKNOWLEDGMENTS

We are grateful to the NSFC (21290171, 21321001, and 21372014) and the National Basic Research Program of China (2013CB933401).

DEDICATION

This work is dedicated to Manfred Scheer for his 60th birthday.

REFERENCES

(1) Ishikawa, N.; Sugita, M.; Ishikawa, T.; Koshihara, S.; Kaizu, Y. *J. Am. Chem. Soc.* **2003**, *125*, 8694−8695.

(2) (a) Wybourne, B. G. *Spectroscopic Properties of Rare Earths*; John Wiley and Sons: New York, 1965. (b) Abragam, A.; Bleaney, B. *Electron Paramagnetic Resonance of Transition Ions*; Oxford University Press: Oxford, U.K., 1970. (c) Marks, T. J. *Chemistry and Spectroscopy of f-Element Organometallics Part I: The Lanthanides*; Wiley: New York, 1978.

(3) (a) Woodruff, D. N.; Winpenny, R. E. P.; Layfield, R. A. *Chem. Rev.* **2013**, *113*, 5110−5148. (b) Layfield, R. A. *Organometallics* **2014**, *33*, 1084−1099. (c) Feltham, H. L. C.; Brooker, S. *Coord. Chem. Rev.* **2014**, *276*, 1−33. (d) Pedersen, K. S.; Bendix, J.; Clerac, R. *Chem. Commun.* **2014**, *50*, 4396−4415.

(4) (a) Pedersen, K. S.; Ungur, L.; Sigrist, M.; Sundt, A.; Schau-Magnussen, M.; Vieru, V.; Mutka, H.; Rols, S.; Weihe, H.; Waldmann, O.; Chibotaru, L. F.; Bendix, J.; Dreiser, J. *Chem. Sci.* **2014**, *5*, 1650−1660. (b) Campbell, V. E.; Bolvin, H.; Rivière, E.; Guillot, R.; Wernsdorfer, W.; Mallah, T. *Inorg. Chem.* **2014**, *53*, 2598−2605.

(5) (a) Jiang, S.-D.; Wang, B.-W.; Su, G.; Wang, Z.-M.; Gao, S. *Angew. Chem., Int. Ed.* **2010**, *49*, 7448−7451. (b) Bi, Y.; Guo, Y.-N.; Zhao, L.; Guo, Y.; Lin, S.-Y.; Jiang, S.-D.; Tang, J.; Wang, B.-W.; Gao, S. *Chem.—Eur. J.* **2011**, *17*, 12476−12481. (c) Li, D.-P.; Wang, T.-W.; Li, C.-H.; Liu, D.-S.; Li, Y.-Z.; You, X.-Z. *Chem. Commun.* **2010**, *46*, 2929−2931. (d) Chen, G.-J.; Gao, C.-Y.; Tian, J.-L.; Tang, J.; Gu, W.; Liu, X.; Yan, S.-P.; Liao, D.-Z.; Cheng, P. *Dalton Trans.* **2011**, *40*, 5579−5583. (e) Li, D.-P.; Zhang, X.-P.; Wang, T.-W.; Ma, B.-B.; Li, C.-H.; Li, Y.-Z.; You, X.-Z. *Chem. Commun.* **2011**, *47*, 6867−6869. (f) Chen, G.-J.; Guo, Y.-N.; Tian, J.-L.; Tang, J.; Gu, W.; Liu, X.; Yan, S.-P.; Cheng, P.; Liao, D.-Z. *Chem.—Eur. J.* **2012**, *18*, 2484−2487. (g) Wang, Z.-G.; Lu, J.; Gao, C.-Y.; Wang, C.; Tian, J.-L.; Gu, W.; Liu, X.; Yan, S.-P. *Inorg. Chem. Commun.* **2013**, *27*, 127−130. (h) Wang, Y.; Li, X.-L.; Wang, T.-W.; Song, Y.; You, X.-Z. *Inorg. Chem.* **2009**, *49*, 969−976. (i) Cosquer, G.; Pointillart, F.; Golhen, S.; Cador, O.; Ouahab, L. *Chem.—Eur. J.* **2013**, *19*, 7895−7903. (j) da Cunha, T. T.; Jung, J.; Boulon, M. E.; Campo, G.; Pointillart, F.; Pereira, C. L.; Guennic, B. L.; Cador, O.; Bernot, K.; Pineider, F.; Golhen, S.; Ouahab, L. *J. Am. Chem. Soc.* **2013**, *135*, 16332−16335.

(6) (a) Jiang, S.-D.; Wang, B.-W.; Sun, H.-L.; Wang, Z.-M.; Gao, S. *J. Am. Chem. Soc.* **2011**, *133*, 4730−4733. (b) Jiang, S.-D.; Liu, S.-S.; Zhou, L.-N.; Wang, B.-W.; Wang, Z.-M.; Gao, S. *Inorg. Chem.* **2012**, *51*, 3079−3087. (c) Meihaus, K. R.; Long, J. R. *J. Am. Chem. Soc.* **2013**, *135*, 17952−17957. (d) Ungur, L.; Le Roy, J. J.; Korobkov, I.; Murugesu, M.; Chibotaru, L. F. *Angew. Chem., Int. Ed.* **2014**, *53*, 4413−4417. (e) Demir, S.; Zadrozny, J. M.; Long, J. R. *Chem.—Eur. J.* **2014**, *20*, 9524−9527. (f) Jeletic, M.; Lin, P.-H.; Le Roy, J. J.; Korobkov, I.; Gorelsky, S. I.; Murugesu, M. *J. Am. Chem. Soc.* **2011**, *133*, 19286−19289. (g) Liu, S.-S.; Ziller, J. W.; Zhang, Y.-Q.; Wang, B.-W.; Evans, W. J.; Gao, S. *Chem. Commun.* **2014**, *50*, 11418−11420.

(7) (a) Harder, S.; Ruspic, C.; Bhriain, N. N.; Berkermanna, F.; Schürmann, M. *Z. Naturforsch.* **2008**, *63b*, 267−274. (b) Shima, T.; Nishiura, M.; Hou, Z. *Organometallics* **2011**, *30*, 2513−2524. (c) Xu, L.; Wang, Z.; Zhang, W.-X.; Xi, Z. *Inorg. Chem.* **2012**, *51*, 11941−11948.

(8) Xi, Z.; Li, P. *Angew. Chem., Int. Ed.* **2000**, *39*, 2950−2952.

(9) *CrysAlisPro Version 1.171.36.28*; Agilent Technologies Inc.: Santa Clara, CA, 2013.

(10) Dolomanov, O. V.; Bourhis, L. J.; Gildea, R. J.; Howard, J. A. K.; Puschmann, H. *J. Appl. Crystallogr.* **2009**, *42*, 339−341.

(11) (a) Oszlanyi, G.; Suto, A. *Acta Crystallogr.* **2004**, *A60*, 134−141. (b) Palatinus, L.; Chapuis, G. *J. Appl. Crystallogr.* **2007**, *40*, 786−790.

(12) Sheldrick, G. M. *Acta Crystallogr.* **2008**, *A64*, 112−122.

(13) Sheldrick, G. M. *SHELXTL 5.10 for Windows NT: Structure Determination Software Programs*; Bruker Analytical X-ray Systems, Inc.: Madison, WI, 1997.

(14) Spek, A. L. *Acta Crystallogr.* **2009**, *D65*, 148−155.

(15) (a) Aquilante, F.; De Vico, L.; Ferré, N.; Ghigo, G.; Malmqvist, P.-å.; Neogrády, P.; Pedersen, T. B.; Pitoňák, M.; Reiher, M.; Roos, B. O.; Serrano-Andrés, L.; Urban, M.; Veryazov, V.; Lindh, R. *J. Comput. Chem.* **2010**, *31*, 224−247. (b) Veryazov, V.; Widmark, P.-O.; Serrano-Andrés, L.; Lindh, R.; Roos, B. O. *Int. J. Quantum Chem.* **2004**, *100*, 626−635. (c) Karlström, G.; Lindh, R.; Malmqvist, P.-Å.; Roos, B. O.; Ryde, U.; Veryazov, V.; Widmark, P.-O.; Cossi, M.; Schimmelpfennig, B.; Neogrady, P.; Seijo, L. *Comput. Mater. Sci.* **2003**, *28*, 222−239.

(16) (a) Kahn, M. L.; Ballou, R.; Porcher, P.; Kahn, O.; Sutter, J.-P. *Chem.—Eur. J.* **2002**, *8*, 525−531. (b) Kahn, M. L.; Sutter, J.-P.; Golhen, S.; Guionneau, P.; Ouahab, L.; Kahn, O.; Chasseau, D. *J. Am. Chem. Soc.* **2000**, *122*, 3413−3421.

(17) (a) Osa, S.; Kido, T.; Matsumoto, N.; Re, N.; Pochaba, A.; Mrozinski, J. *J. Am. Chem. Soc.* **2004**, *126*, 420−421. (b) Gao, Y.; Xu, G.-F.; Zhao, L.; Tang, J.; Liu, Z. *Inorg. Chem.* **2009**, *48*, 11495−11497.

(18) Abbas, G.; Lan, Y. H.; Kostakis, G. E.; Wernsdorfer, W.; Anson, C. E.; Powell, A. K. *Inorg. Chem.* **2010**, *49*, 8067−8072.

(19) (a) Cole, K. S.; Cole, R. H. *J. Chem. Phys.* **1941**, *9*, 341−352. (b) Aubin, S. M. J.; Sun, Z.; Pardi, L.; Krzystek, J.; Folting, K.; Brunel, L.-C.; Rheingold, A. L.; Christou, G.; Hendrickson, D. N. *Inorg. Chem.* **1999**, *38*, 5329−5340.

(20) (a) Shrivastava, K. N. *Phys. Status Solidi B* **1983**, *117*, 437−458. (b) Brya, W. J.; Wagner, P. E. *Phys. Rev.* **1966**, *147*, 239−241. (c) Hoffmann, S. K.; Hilczer, W.; Goslar, J.; Augustyniak-Jablokow, M. A. *J. Phys.: Condens. Matter* **2001**, *13*, 7443−7457.

(21) Malmqvist, P. Å.; Roos, B. O.; Schimmelpfennig, B. *Chem. Phys. Lett.* **2002**, *357*, 230−240.

(22) (a) Bernot, K.; Luzon, J.; Bogani, L.; Etienne, M.; Sangregorio, C.; Shanmugam, M.; Caneschi, A.; Sessoli, R.; Gatteschi, D. *J. Am. Chem. Soc.* **2009**, *131*, 5573−5579. (b) Cucinotta, G.; Perfetti, M.; Luzon, J.; Etienne, M.; Car, P.-E.; Caneschi, A.; Calvez, G.; Bernot, K.; Sessoli, R. *Angew. Chem., Int. Ed.* **2012**, *51*, 1606−1610. (c) Boulon, M.-E.; Cucinotta, G.; Luzon, J.; Degl'Innocenti, C.; Perfetti, M.; Bernot, K.; Calvez, G.; Caneschi, A.; Sessoli, R. *Angew. Chem., Int. Ed.* **2013**, *52*, 350−354. (d) Boulon, M.-E.; Cucinotta, G.; Liu, S.-S.; Jiang, S.-D.; Ungur, L.; Chibotaru, L. F.; Gao, S.; Sessoli, R. *Chem.—Eur. J.* **2013**, *19*, 13726−13731.

(23) Chilton, N. F.; Collison, D.; McInnes, E. J. L.; Winpenny, R. E. P.; Soncini, A. *Nat. Commun.* **2013**, *4*, 2551−2557.

(24) Baldoví, J. J.; Cardona-Serra, S.; Clemente-Juan, J. M.; Coronado, E.; Gaita-Ariño, A.; Palii, A. *J. Comput. Chem.* **2013**, *34*, 1961−1967.

(25) Sievers, J. *Z. Phys. B: Condens. Matter* **1982**, *45*, 289−296.

(26) Aravena, D.; Ruiz, E. *Inorg. Chem.* **2013**, *52*, 13770−13778.

(27) Barra, A. L.; Caneschi, A.; Cornia, A.; Gatteschi, D.; Gorini, L.; Heiniger, L. P.; Sessoli, R.; Sorace, L. *J. Am. Chem. Soc.* **2007**, *129*, 10754−10762.

(28) (a) Rinehart, J. D.; Long, J. R. *Chem. Sci.* **2011**, *2*, 2078−2085. (b) Baldoví, J. J.; Cardona-Serra, S.; Clemente-Juan, J. M.; Coronado, E.; Gaita-Ariño, A.; Palii, A. *Inorg. Chem.* **2012**, *51*, 12565−12574.

DOI: 10.1021/ic502734z
Inorg. Chem. 2015, 54, 5162−5168